Numerical boundary conditions for globally mass conservative methods to solve the shallow-water equations and applied to river flow

J. Burguete[‡], P. García-Navarro[*,†] and J. Murillo[§]

Fluid Mechanics, CPS, University of Zaragoza, Zaragoza, Spain

SUMMARY

A revision of some well-known discretization techniques for the numerical boundary conditions in 1D shallow-water flow models is presented. More recent options are also considered in the search for a fully conservative technique that is able to preserve the good properties of a conservative scheme used for the interior points. Two conservative numerical schemes are used as representatives of the families of explicit and implicit numerical methods. The implementation of the different boundary options to these schemes is compared by means of the simulation of several test cases with exact solution. The schemes with the global conservation boundary discretization are applied to the simulation of a real river flood wave leading to very satisfactory results. Copyright © 2005 John Wiley & Sons, Ltd.

1. INTRODUCTION

This work deals essentially with the discrete representation of the boundary conditions in the context of 1D shallow-water flow problems. This is a minor section in most of the reference papers but, in the present work, the emphasis is put on the influence, that a careless method at the boundaries can have on the global numerical solution.

It is well known that conservative methods are the best option for the numerical solution of conservation laws. These methods furnish a good discrete representation in which all the inter-cell contributions cancel out so that the only variations are due to source terms and flow at the boundaries. In order to reach the correct numerical solution in a general unsteady case, it is clear that the numerical scheme chosen for the interior points is as important as

---

*Correspondence to: P. García-Navarro, Área de Mecánica de Fluidos, Centro Politécnico Superior, Universidad de Zaragoza, c/María de Luna 3, 50018 Zaragoza, Spain.
†E-mail: pigar@unizar.es
‡E-mail: jburguete@able.es
§E-mail: jmurillo@mafalda.cps.unizar.es

the source term treatment and the method applied to discretize the boundary conditions. The question of the best options to deal with the source terms has previously been treated for instance in References [1–5].

As for the boundary conditions, the starting point is the theory of characteristics. It provides a clear idea of the space–time directions followed by the information, of the influence regions and of the required number of boundary conditions to have a well-posed problem [6]. When, in the x–t plane, a characteristic curve enters the computational domain, the region of influence is exterior to the domain and an additional condition is required. This is called a physical boundary condition. On the other hand, if the curve leaves the domain, the region of influence falls within the computational domain and the boundary condition depends exclusively on the interior variables. As inlet and outlet boundary points represent a cut-off of the domain, one would like to solve the governing equations using the same scheme even at the boundary. However, the basic scheme must be adapted to the fact that only the interior points can be involved in this calculation. These are called numerical boundary conditions, not actual boundary conditions, and their correct discrete representation is the main objective of this work.

Hartree, according to Fox [7], proposed an iterative method based on linear interpolation of the Riemann invariants. The methods of characteristic variable extrapolation (CVE), applied originally in fluid mechanics by Yee *et al.* [8, 9], are much simpler and lead to similar results. Even simpler approaches for the 1D model are the methods based on the local mass conservation equation, proposed by Jin and Fread [10], leading to similar results as shown by Villanueva [11] in several examples in rivers and irregular channels.

All the methods proposed in the past to discretize the numerical boundary conditions generate error in the global mass conservation (GMC). In this work, a method based on the integral form of the mass conservation equation extended to the full domain (GMC) is also considered. It was first introduced in References [4, 5, 12] and preliminarily used. The technique can be adapted to any conservative numerical scheme used for the interior points leading to a machine accuracy GMC in all steady or unsteady situations. As an example, the technique will be derived for both, an explicit and an implicit conservative method, using them as representative of the two main families of numerical schemes in 1D models. In both cases this technique is sensitive to the time step size in presence of unsteady discontinuous boundary conditions. A correction strategy to avoid numerical difficulties in these cases is suggested.

Four different methods to discretize the numerical conditions are detailed and their performance is compared using a few test cases with analytical solution. Some of these test cases involve unsteady discontinuous boundary conditions and some of them deal with steady continuous flow. The best option is chosen and applied finally to a river flow test case.

2. BASIC EQUATIONS

One-dimensional shallow-water flows can be modelled by means of the Saint-Venant equations [13]. The conservative form of such equations admits a vectorial expression as follows:

$$\frac{\partial \mathbf{u}(x,t)}{\partial t} + \frac{\mathrm{d}\mathbf{F}^c(x,\mathbf{u})}{\mathrm{d}x} = \mathbf{S}^c(x,\mathbf{u}) \tag{1}$$

with $\mathbf{u}$ the vector of conserved variables, $\mathbf{F}^c$ the fluxes and $\mathbf{S}^c$ the source terms:

$$\mathbf{u} = \begin{pmatrix} A \\ Q \end{pmatrix}, \quad \mathbf{F}^c = \begin{pmatrix} Q \\ \dfrac{Q^2}{A} + gI_1 \end{pmatrix}, \quad \mathbf{S}^c = \begin{pmatrix} 0 \\ g\left[I_2 + A(S_0 - S_\mathrm{f})\right] \end{pmatrix} \tag{2}$$

where A is the wetted cross section, Q the discharge, g the acceleration constant of gravity, S_0 the bed slope and S_f the friction slope that is commonly modelled with the Gauckler–Manning law [14, 15]:

$$S_\mathrm{f} = \frac{n^2 Q|Q|P^{4/3}}{A^{10/3}} \tag{3}$$

In this friction law n is the Manning's roughness coefficient and P is the wetted perimeter. Furthermore, I_1 and I_2 represent the pressure forces:

$$I_1 = \int_0^h \sigma(x, z')(h - z')\,\mathrm{d}z', \quad I_2 = \int_0^h \frac{\partial \sigma(x, z')}{\partial x}(h - z')\,\mathrm{d}z' \tag{4}$$

where h is the water depth and σ is the cross-section width at a distance z' of the section bottom.

The integrals of the conservative form are difficult to deal with, in general. They can be eliminated by transformation of the above system into the quasi-conservative form [4]:

$$\frac{\partial \mathbf{u}(x, t)}{\partial t} + \frac{\partial \mathbf{F}^{qc}(\mathbf{u})}{\partial x} = \mathbf{S}^{qc}(x, \mathbf{u}) \tag{5}$$

being $\mathbf{F}^{qc}$ and $\mathbf{S}^{qc}$, respectively, the flux and source terms of the quasi-conservative form of the equations:

$$\mathbf{F}^{qc} = \begin{pmatrix} Q \\ \dfrac{Q^2}{A} \end{pmatrix}, \quad \mathbf{S}^{qc} = \begin{pmatrix} 0 \\ -gA\left(\dfrac{\partial z_s}{\partial x} + S_\mathrm{f}\right) \end{pmatrix} \tag{6}$$

with z_s the vertical coordinate of the free surface.

From the conservative form (1), it is possible to derive a non-conservative form by developing the spatial derivative [3]:

$$\frac{\partial \mathbf{u}(x, t)}{\partial t} + \mathbf{J}(x, \mathbf{u})\frac{\partial \mathbf{u}(x, t)}{\partial x} = \mathbf{S}^{nc}(x, \mathbf{u}) \tag{7}$$

where $\mathbf{J} = \partial \mathbf{F}^c / \partial \mathbf{u}$ is the Jacobian of the conservative flux and $\mathbf{S}^{nc} = \mathbf{S}^c - (\partial \mathbf{F}^c / \partial x)$ is the source term of the non-conservative form:

$$\mathbf{J} = \begin{pmatrix} 0 & 1 \\ c^2 - u^2 & 2u \end{pmatrix}, \quad \mathbf{S}^{nc} = \begin{pmatrix} 0 \\ -gA\left(\dfrac{\partial z_s}{\partial x} + S_\mathrm{f}\right) + c^2 \dfrac{\partial A}{\partial x} \end{pmatrix} \tag{8}$$

Here B is the wetted cross-section top width, $u = Q/A$ is the flow velocity and $c = \sqrt{g(A/B)}$ is the speed of the small surface waves.

The non-conservative equations (7) can be decoupled if the Jacobian is diagonalized and a set of independent equations is obtained. Let $\mathbf{P}$ be the matrix that makes diagonal the flux Jacobian $\mathbf{J}$. This matrix is made of the eigenvectors of $\mathbf{J}$ so that

$$\mathbf{J} = \mathbf{P}\mathbf{\Lambda}\mathbf{P}^{-1}, \quad \mathbf{\Lambda} = \mathbf{P}^{-1}\mathbf{J}\mathbf{P} \tag{9}$$

with $\mathbf{\Lambda}$ the diagonal matrix with the $\mathbf{J}$'s eigenvalues on the diagonal. In our model

$$\mathbf{P} = \begin{pmatrix} 1 & 1 \\ u+c & u-c \end{pmatrix}, \quad \mathbf{P}^{-1} = \frac{1}{2c}\begin{pmatrix} c-u & 1 \\ c+u & -1 \end{pmatrix}, \quad \mathbf{\Lambda} = \begin{pmatrix} u+c & 0 \\ 0 & u-c \end{pmatrix} \tag{10}$$

The characteristic variables $\mathbf{w}$ are defined according to the following property at the differential level:

$$\mathrm{d}\mathbf{w} = \mathbf{P}^{-1}\,\mathrm{d}\mathbf{u} = \frac{1}{2c}\begin{pmatrix} (c-u)\mathrm{d}A + \mathrm{d}Q \\ (c+u)\mathrm{d}A - \mathrm{d}Q \end{pmatrix} \tag{11}$$

Using this into (7), the characteristic form of the equations can be obtained:

$$\frac{\partial\mathbf{w}(x,t)}{\partial t} + \mathbf{\Lambda}(x,\mathbf{w})\frac{\partial\mathbf{w}(x,t)}{\partial x} = \mathbf{P}^{-1}(x,\mathbf{w})\mathbf{S}^{nc}(x,\mathbf{w}) \tag{12}$$

It is worth noting that the characteristic variables are not defined, in general, since, unless for linear systems, it is not possible to find a set of variables holding (11). However, it is possible to use their differences and refer to them as a combination of the differences of the conserved variables.

The differential forms of the shallow-water equations (1), (5), (7) or (12), are equivalent and all valid for problems with differentiable and continuous solutions but they all fail in cases with non-differentiable or discontinuous solutions. In these cases, the mass and momentum conservation equations must be formulated in integral form:

$$\int_{x_0}^{x_0+\Delta x} [\mathbf{u}(x,t_0+\Delta t) - \mathbf{u}(x,t_0)]\,\mathrm{d}x + \int_{t_0}^{t_0+\Delta t} [\mathbf{F}^i(x_0+\Delta x,t) - \mathbf{F}^i(x_0,t)]\,\mathrm{d}t$$

$$= \int_{t_0}^{t_0+\Delta t} \mathbf{S}^i(t)\,\mathrm{d}t \tag{13}$$

with $\mathbf{F}^i$ and $\mathbf{S}^i$, respectively, the flux and source terms of the integral form. In the 1D shallow-water flow model with cross-sectional average, these are:

$$\mathbf{F}^i = \begin{pmatrix} Q \\ \dfrac{Q^2}{A} + gI_1 \end{pmatrix}, \quad \mathbf{S}^i = \begin{pmatrix} 0 \\ \displaystyle\int_{S_b} [ghn_{bx} + \tau_b]\,\mathrm{d}S_b \end{pmatrix} \tag{14}$$

with S_b representing the solid surface in the control volume and n_{bx} the x component of its normal vector. This is the most general form of the equations and is valid for problems with discontinuous solution.

The flow equations in integral form (13) can be used to model flows involving discontinuities. If the discontinuity is located at x_0 at time t_0 and the reference system is chosen to

move at the instantaneous speed of propagation of the discontinuity U, the integral equations for a volume centred around x_0 are

$$\int_{x_0-(\Delta x/2)}^{x_0+(\Delta x/2)} [A(x, t_0 + \Delta t) - A(x, t_0)] \mathrm{d}x$$

$$+ \int_{t_0}^{t_0+\Delta t} \left[Q\left(x_0 + \frac{\Delta x}{2}, t\right) - Q\left(x_0 - \frac{\Delta x}{2}, t\right) \right] \mathrm{d}t = 0$$

$$\int_{x_0-(\Delta x/2)}^{x_0+(\Delta x/2)} [Q(x, t_0 + \Delta t) - Q(x, t_0)] \mathrm{d}x + \int_{t_0}^{t_0+\Delta t} \left[\left(\frac{Q^2}{A} + gI_1 \right)_{x_0+(\Delta x/2), t} \right.$$

$$\left. - \left(\frac{Q^2}{A} + gI_1 \right)_{x_0-(\Delta x/2), t} \right] \mathrm{d}t = \int_{t_0}^{t_0+\Delta t} \mathrm{d}t \left\{ \int_{S_b(t)} [ghn_{bx} + \tau_b]_{x, y, t} \, \mathrm{d}S_b \right.$$

$$\left. + \int_{x_0-(\Delta x/2)}^{x_0+(\Delta x/2)} A(x, t) \frac{\partial U(t)}{\partial t} \, \mathrm{d}x \right\} \tag{15}$$

The last term appears since the moving reference can be non-inertial. By seeking the limit when Δx tends to zero, the integrals of the functions between $x_0 - (\Delta x/2)$ and $x_0 + (\Delta x/2)$ disappear and the contribution of the friction forces on the element cancels out, leading to the following equations of shock propagation in the moving reference system:

$$\delta(Au) = 0$$

$$\delta(Au^2 + gI_1) = \int_{S_b(t)} [ghn_{bx}]_{x, y, t} \, \mathrm{d}S_b \tag{16}$$

δf represents the change in f across the discontinuity. The integral over the solid surface will only be different from zero when the bed is discontinuous at x_0 (a bottom step or a sudden contraction/expansion), since only then the solid surface S_b will have a non-infinitesimal value along Δx. In that case the integral represents the x component of the pressure force on the obstacle. If the solid bed is continuous, going back to the absolute reference system, the following equations are obtained for the flow discontinuity:

$$\delta[A(u - U)] = 0$$

$$\delta[A(u - U)^2 + gI_1] = 0 \tag{17}$$

These are the shallow-water flow version of the Rankine–Hugoniot [16] equations for 1D shocks in fluids.

3. NUMERICAL SCHEMES

Having stated that our main goal is the derivation of a globally exact conservative scheme for the shallow-water equations, conservative numerical methods are required both for the interior

and the boundary points. This section is devoted to that challenge. The following vector is defined:

$$\mathbf{G}_{i+(1/2)} \equiv \left(\mathbf{S}^c - \frac{\delta \mathbf{F}^c}{\delta x}\right)_{i+(1/2)} = \left(\mathbf{S}^{qc} - \frac{\delta \mathbf{F}^{qc}}{\delta x}\right)_{i+(1/2)} = \left(\mathbf{S}^{nc} - \mathbf{J}\frac{\delta \mathbf{u}}{\delta x}\right)_{i+(1/2)} \tag{18}$$

using the notation $\delta f_{i+(1/2)} = f_{i+1} - f_i$, $f_{i+(1/2)} = (f_{i+1} + f_i)/2$ so that the conservative, quasi-conservative and non-conservative forms are equivalent. In order to enforce the two conditions involved in that equivalence it is necessary to also define:

$$(gI_2)_{i+(1/2)} = \left(\frac{\delta I_1}{\delta x} - A\frac{\delta h}{\delta x}\right)_{i+(1/2)}$$

$$\tilde{u}_{i+(1/2)} = \frac{Q_{i+1}/\sqrt{A_{i+1}} + Q_i/\sqrt{A_i}}{\sqrt{A_{i+1}} + \sqrt{A_i}}, \quad \tilde{c}_{i+(1/2)} = \sqrt{g\frac{A_{i+(1/2)}}{B_{i+(1/2)}}} \tag{19}$$

These average values, proposed in References [2, 4], are an extension of the Roe's average [17] to hyperbolic equations with source terms having explicit spatial dependence. They lead to identical results either using the conservative, quasi-conservative or non-conservative form of the equations. For the sake of simplicity, however, the quasi-conservative form will be used in this work [4].

When a semi-implicit treatment of source term is made:

$$\mathbf{S} \approx \theta \mathbf{S}^{n+1} + (1 - \theta)\mathbf{S}^n \approx \mathbf{S}^n + \theta \mathbf{K}^n \Delta \mathbf{u}^n \tag{20}$$

where $\theta \in [0, 1]$ is an implicit parameter for the source term and $\mathbf{K} = \partial \mathbf{S}/\partial \mathbf{u}$ is the source term Jacobian:

$$\mathbf{K} = \begin{pmatrix} 0 & 0 \\ -g\left[\frac{\partial z_s}{\partial x} - \frac{1}{B}\frac{\partial A}{\partial x} + S_f\left(\frac{4A}{3P}\frac{\partial P}{\partial A} - \frac{7}{3}\right)\right] & -\frac{2gS_f}{u} \end{pmatrix} \tag{21}$$

then, conservative schemes with non-pointwise source term can be formulated in the form of a wave decomposition as [3]:

$$(1 - \theta\Delta t\mathbf{K}_i^n)\Delta \mathbf{u}_i^n = \Delta t(\mathbf{G}_{i+(1/2)}^{\mathrm{R}} + \mathbf{G}_{i-(1/2)}^{\mathrm{L}}) \tag{22}$$

where $\mathbf{G}_{i+(1/2)}^{\mathrm{R,L}}$ represent the particular decomposition of every scheme. This kind of numerical scheme is conservative as long as a nodal numerical flux $\mathbf{F}_i^{\mathrm{T}}$ can be defined so that [3]:

$$\mathbf{F}_{i+1}^{\mathrm{T}} - \mathbf{F}_i^{\mathrm{T}} = \delta\mathbf{F}_{i+(1/2)}^{\mathrm{R}} + \delta\mathbf{F}_{i+(1/2)}^{\mathrm{L}} \tag{23}$$

Two numerical schemes will be next outlined as the best candidates of the families of explicit and implicit conservative schemes. The necessary steps to implement all the boundary methods considered in this work will be described. From our previous experience, the second-order upwind TVD explicit scheme has been chosen as the most accurate and the first-order upwind semi-explicit scheme has been selected for the property of being the only scheme able to deal with non-linear shock propagation at high CFL numbers.

3.1. Second-order TVD scheme

A second-order in space and time TVD scheme with non-pointwise source term as proposed in Reference [3] will be used in this work. It is an extension of the method proposed by Glaister [1] to improve the second-order TVD scheme [18]. The upwind decomposition is defined as

$$\mathbf{A}^{\pm} = \mathbf{P}\mathbf{\Omega}^{\pm}\mathbf{P}^{-1}\mathbf{A} \tag{24}$$

with $\mathbf{A}$ a general matrix and

$$\mathbf{\Omega}^{\pm} = \begin{pmatrix} \frac{1}{2}[1 \pm \operatorname{sign}(\lambda_1)] & 0 \\ 0 & \frac{1}{2}[1 \pm \operatorname{sign}(\lambda_2)] \end{pmatrix} \tag{25}$$

where $\lambda_1 = u + c$, $\lambda_2 = u - c$ are the eigenvalues of the Jacobian matrix (8). At the same time, the following second-order vectors are defined:

$$\mathbf{H}^{\pm} = \left(1 \mp \frac{\Delta t}{\Delta x}\mathbf{J}^{\pm}\right)\mathbf{G}^{\pm} \tag{26}$$

so that the influence of the positive $(+)$ and negative $(-)$ eigenvalues is separated, and the second-order TVD is formulated as [3]

$$(1 - \tfrac{1}{2}\Delta t \mathbf{K}_i^n)\Delta \mathbf{u}_i^n = \Delta t[(\mathbf{G}^+)_{i-(1/2)}^n + (\mathbf{G}^-)_{i+(1/2)}^n]$$

$$+ \frac{\Delta t}{2}[(\mathbf{\Psi}^+\mathbf{H}^+)_{i-(1/2)}^n + (\mathbf{\Psi}^-\mathbf{H}^-)_{i+(1/2)}^n - (\mathbf{\Psi}^+\mathbf{H}^+)_{i-(3/2)}^n - (\mathbf{\Psi}^-\mathbf{H}^-)_{i+(3/2)}^n] \tag{27}$$

where $\mathbf{\Psi}^{\pm}$ are the flux-limiting diagonal matrices [3]:

$$(\mathbf{\Psi}^{\pm})_{i+(1/2)}^n = \begin{pmatrix} \psi\left(\dfrac{[(\mathbf{H}^{\pm})^1]_{i+(1/2)\pm1}^n}{[(\mathbf{H}^{\pm})^1]_{i+(1/2)}^n}\right) & & \\ & \ddots & \\ & & \psi\left(\dfrac{[(\mathbf{H}^{\pm})^k]_{i+(1/2)\pm1}^n}{[(\mathbf{H}^{\pm})^k]_{i+(1/2)}^n}\right) \end{pmatrix} \tag{28}$$

with $(\mathbf{H}^{\pm})^k$ the k component of the vectors $\mathbf{H}^{\pm}$ and ψ the flux-limiting function. In this work the following will be used:

- Minmod [19]: $\psi(r) = \max[0, \min(1, r)]$.

In transitions from subcritical to supercritical flow, the above scheme (28) can enforce non-physical discontinuities. To avoid this problem, the first-order terms can be redefined with no alteration of the second-order terms $\mathbf{H}^{\pm}$ [4]:

$$(\mathbf{G}^{\pm})_{i+(1/2)}^n = \left\{ \mathbf{P}\mathbf{\Omega}^{\pm}\mathbf{P}^{-1}\mathbf{G} \mp \frac{1}{4}\max_k(v^k)\frac{\delta \mathbf{u}}{\delta x} \right\}_{i+(1/2)}^n \tag{29}$$

with:

$$(v^k)^n_{i+(1/2)} = \begin{cases} [\delta(\lambda^k) - |\tilde{\lambda}^k|]^n_{i+(1/2)} & \text{if } (\lambda^k)^n_i < 0 \text{ and } (\lambda^k)^n_{i+1} > 0 \\ 0 & \text{otherwise} \end{cases} \tag{30}$$

this represents an additional viscosity, formulated in a simple form and able to be adapted to both explicit and implicit schemes. For more details see References [3–5]. The second-order TVD scheme with upwind source term is a conservative scheme and admits the following wave decomposition (WD) [3]:

$$\mathbf{F}^{\mathrm{T}}_i = \mathbf{F}^n_i, \quad \mathbf{G}^{\mathrm{R}}_{i+(1/2)} = (\mathbf{G}^-)^n_{i+(1/2)} + \tfrac{1}{2}[(\mathbf{\Psi}^+\mathbf{H}^+)^n_{i-(1/2)} - (\mathbf{\Psi}^-\mathbf{H}^-)^n_{i+(3/2)}]$$

$$\mathbf{G}^{\mathrm{L}}_{i+(1/2)} = (\mathbf{G}^+)^n_{i+(1/2)} - \tfrac{1}{2}[(\mathbf{\Psi}^+\mathbf{H}^+)^n_{i-(1/2)} - (\mathbf{\Psi}^-\mathbf{H}^-)^n_{i+(3/2)}] \tag{31}$$

being also TVD and stable provided that [3]:

$$\mathrm{CFL} \leqslant 1 \tag{32}$$

with CFL the Courant–Friedrichs–Lewy dimensionless number [20]. For the 1D shallow-water flow model this is

$$\mathrm{CFL} = \Delta t \max_i \left(\frac{|u| + c}{\Delta x} \right)^n_i \tag{33}$$

3.2. First-order bidiagonal semi-explicit scheme

This is a two-step numerical scheme proposed in Reference [5], that can be outlined as

$$[(1 + \xi^-)\Delta\mathbf{u}^-]^n_i - (\xi^-\Delta\mathbf{u}^-)^n_{i+1} = \Delta t(\mathbf{G}^-)^n_{i+(1/2)}$$

$$[(1 + \xi^+)\Delta\mathbf{u}^+]^n_i - (\xi^+\Delta\mathbf{u}^+)^n_{i-1} = \Delta t(\mathbf{G}^+)^n_{i-(1/2)} \tag{34}$$

$$(1 - \theta\Delta t\mathbf{K}^n_i)\Delta\mathbf{u}^n_i = (\Delta\mathbf{u}^+ + \Delta\mathbf{u}^-)^n_i$$

with $\mathbf{G}^\pm$ defined as in (29) and the parameters $\xi^\pm$ as in Reference [5]:

$$\xi^\pm_i = \max \left[\pm\frac{\Delta t}{\Delta x}(\lambda^\pm)^n_i - 0.9, \xi^\pm_{i\pm1} - 0.9, 0 \right] \tag{35}$$

where

$$\lambda^+ = \max_k(\lambda^k, 0), \quad \lambda^- = \min_k(\lambda^k, 0) \tag{36}$$

and the following correction to avoid boundary instability in a grid with N cells:

$$\xi^+_1 = \xi^-_N = \max(\mathrm{CFL} - 0.9, 0) \tag{37}$$

The scheme so defined is unconditionally stable. This definition involves a minor and stabilizing correction to the formerly proposed in Reference [5].

The scheme is conservative with a WD [5]:

$$\mathbf{F}_i^{\mathrm{T}} = \mathbf{F}_i^n + \frac{\Delta x}{\Delta t}(\xi^+ \Delta \mathbf{u}^+ - \xi^- \Delta \mathbf{u}^-)_i^n$$

$$\mathbf{G}_{i+(1/2)}^{\mathrm{R}} = (\mathbf{G}^-)_{i+(1/2)}^n + \frac{1}{\Delta t}[(\xi^- \Delta \mathbf{u}^-)_{i+1}^n - (\xi^- \Delta \mathbf{u}^-)_i^n]$$

$$\mathbf{G}_{i+(1/2)}^{\mathrm{L}} = (\mathbf{G}^+)_{i+(1/2)}^n - \frac{1}{\Delta t}[(\xi^+ \Delta \mathbf{u}^+)_{i+1}^n - (\xi^+ \Delta \mathbf{u}^+)_i^n] \qquad (38)$$

The method as defined here is open to different options for the increments $(\Delta \mathbf{u}^+)_1^n$ and $(\Delta \mathbf{u}^-)_N^n$ at the boundaries. They must contain the information corresponding to the physical (external) boundary conditions. As an example, if the inlet discharge Q^* is the imposed upstream boundary condition, the following will be written:

$$\Delta Q_1^+ = Q^* - Q_1^n \qquad (39)$$

4. BOUNDARY CONDITIONS

A correct numerical model for unsteady flow problems must be based not only on a numerical scheme with good properties, but also on an adequate procedure to discretize the boundary conditions. The theory of characteristics provides clear indications about the number of necessary external boundary conditions to define a well-posed problem [6]. As Figure 1 illustrates, when a characteristic curve defined in the x–t plane enters the computational domain, the influence region associated to it is exterior to the domain, and therefore one external boundary condition is required. This kind of boundary conditions is also called physical boundary conditions. On the other hand, when the characteristic curve leaves the domain, the influence region belongs to the computational domain and the information linked to that characteristic curve depends exclusively on the interior points. This kind of boundary conditions are also called numerical boundary conditions.

The speeds of propagation of information and the regions of influence in the x–t plane can be obtained from the differential characteristic form of Equations (12). These are a set of
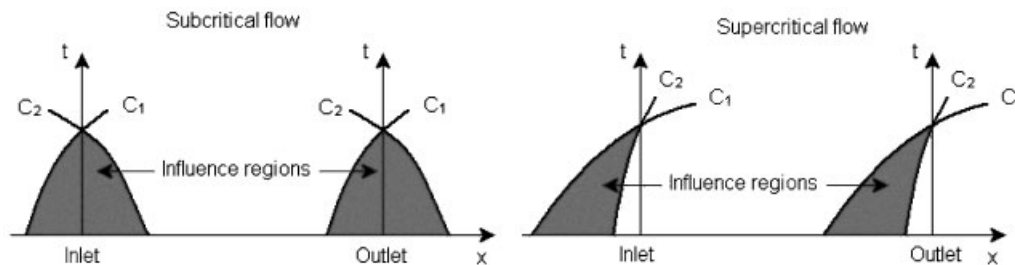

Figure 1. Influence regions at the inlet and at the outlet for both subcritical and supercritical flows.

equations in the form

$$\frac{\partial w_i}{\partial t} + \lambda_i \frac{\partial w_i}{\partial x} = \beta_i \tag{40}$$

where λ_i are the propagation speeds. In the 1D shallow-water system they correspond to the eigenvalues of the Jacobian matrix (8):

$$\lambda_1 = u + c, \quad \lambda_2 = u - c \tag{41}$$

These velocities can be used to define the characteristic curves bounding the regions of influence of a given point on the x–t plane. In the 1D shallow-water model there are two characteristic curves at every point. In regions of left to right supercritical flow ($u > c$) both curves have a positive slope ($\lambda_1 > 0$, $\lambda_2 > 0$), and hence two physical boundary conditions are required at the inlet and two numerical boundary conditions are required at the outlet. However, in case of subcritical flow, one curve has positive slope ($\lambda_1 > 0$) and the other a negative slope ($\lambda_2 < 0$), requiring both physical and numerical boundary conditions at the inlet and the outlet.

The most usual physical boundary conditions at the inlet are a discharge hydrograph $Q(t)$ or a water depth limnigraph $h(t)$ in case of subcritical flow and both together $Q(t)$, $h(t)$ in case of supercritical flow. Only in case of subcritical flow, and only one physical boundary condition is necessary at the outlet, being the most common practice to use a rating curve of the type $Q = Q(h)$ or a limnigraph $h(t)$. Critical outlet or closed outlet can be considered particular cases.

Numerical boundary conditions are those additional equations required to enable the correct numerical resolution at the boundary points. They carry some kind of information from the calculation domain. One of the most important mathematical properties concerning the methods for numerical boundary conditions, established by Gustafsson [21], states that they can be up to one order of approximation less than the numerical scheme used for the interior points and still preserve the global accuracy. Therefore, first-order methods can be applied to the boundary conditions when dealing with second-order methods for the rest of the points, and zero-order methods in case of using a first-order numerical scheme.

4.1. Stabilization correction

It is important to remark that discontinuous boundary conditions can violate the stability condition (33) due to sudden changes in u and c. When dealing with supercritical flows, 2 variables, A^* and Q^*, are imposed at the inlet, forcing therefore the values of u^* and c^*. In order to avoid stability problems we shall define from (33) the size of the time step as

$$\Delta t = \text{CFL} \min_i \left(\frac{\Delta x}{|u|_i^n + c_i^n}, \frac{\Delta x}{|u|^* + c^*} \right) \tag{42}$$

In case of subcritical flow, only one of the variables, A^* or Q^*, is imposed as physical boundary condition. In order to avoid possible instabilities let us assume the worst case, that of critical flow:

$$u^* = c^* \Rightarrow \frac{g A^{*3}}{B^*} = Q^{*2} \tag{43}$$

This equation is explicit if A^* is known, and can be approximated if Q^* is known. Once the values of u^* and c^* at the boundary are estimated (42) can be applied.

4.2. Characteristic variable extrapolation (CVE)

There exist several methods based on characteristics. Among them, the most commonly used are those of CVE. For instance, the first-order spatial extrapolation:

$$\delta w_{i+(1/2)}^{n+1} = \delta w_{i+(3/2)}^{n+1} \tag{44}$$

valid, as stated before, to complement methods of first and second order. For first-order methods the even simpler zero-order version can also be used:

$$\delta w_{i+(1/2)}^{n+1} = 0 \tag{45}$$

The conditions to be met by the variable extrapolation methods and different numerical schemes to preserve linear stability were generalized by Kreiss [22] and by Gustafsson *et al.* [23] and were later applied by Yee *et al.* [8, 9] to fluid mechanics equations.

   As an example, we shall consider the first-order spatial extrapolation method in the context of the shallow-water equations. In subcritical flow, the second differential characteristic equation (12) is to be used as numerical boundary condition at the inlet since it is associated to a negative characteristic slope. Using the extrapolation of the differential characteristic variable:

$$\left\{ \frac{1}{2c} [(c+u)\delta A - \delta Q] \right\}_{(3/2)}^{n+1} = \left\{ \frac{1}{2c} [(c+u)\delta A - \delta Q] \right\}_{(5/2)}^{n+1} \tag{46}$$

At the outlet, the first differential characteristic variable must be used due to the associated positive slope, that is

$$\left\{ \frac{1}{2c} [(c-u)\delta A + \delta Q] \right\}_{N-(1/2)}^{n+1} = \left\{ \frac{1}{2c} [(c-u)\delta A + \delta Q] \right\}_{N-(3/2)}^{n+1} \tag{47}$$

The following linearization is usually applied in order to simplify the resolution:

$$u_{i+(1/2)}^{n+1} \approx u_{i+(1/2)}^{n}, \quad c_{i+(1/2)}^{n+1} \approx c_{i+(1/2)}^{n} \tag{48}$$

where c and u can be defined using the Roe's averages (19).

   Expressions (46) and (47) are simpler in case of using the zero-order version:

$$[(c+u)\delta A - \delta Q]_{(3/2)}^{n+1} = 0, \quad [(c-u)\delta A + \delta Q]_{N-(1/2)}^{n+1} = 0 \tag{49}$$

   The bidiagonal upwind scheme, as defined in (34), is open to the definition of the increments $(\Delta \mathbf{u}^+)_1^n$ and $(\Delta \mathbf{u}^-)_N^n$. From the information supplied by the physical boundary condition, the zero-order temporal extrapolation of the variables can be used as follows:

$$[(c+u)\Delta A^+ - \Delta Q^+]_1^n = 0, \quad [(c-u)\Delta A^- + \Delta Q^-]_N^n = 0 \tag{50}$$

4.3. Wave decomposition (WD)

In Reference [3], a hybrid scheme was proposed based on conservative and characteristic methods. A conservative numerical scheme is first applied neglecting the possible contributions from cells external to the calculation domain, for instance,

$$(\mathbf{G}^{\pm})_j^n = (\mathbf{H}^{\pm})_j^n = 0 \quad \text{if } j < 1 \text{ or } j > N \tag{51}$$

in the considered schemes and with the correction at the boundaries described in (49). The numerical increments in the variables obtained after this first step will be called $\Delta\mathbf{u}_i^p$. It is possible to get a relationship between the physical increments $\Delta\mathbf{u}_i^n$ assuming constant the associated characteristic variable, as in the extrapolation methods described in the previous subsection:

$$\Delta w^n = \Delta w^p \tag{52}$$

This method is of first order.

As in the CVE methods, in case of subcritical flow the second characteristic variable (12) must be used at the inlet due to the negative propagation speed:

$$(c + u)_1^n \Delta A_1^n - \Delta Q_1^n = (c + u)_1^n \Delta A_1^p - \Delta Q_1^p \tag{53}$$

and the first characteristic variable at the outlet due to the associated positive propagation speed:

$$(c - u)_N^n \Delta A_N^n + \Delta Q_N^n = (c - u)_N^n \Delta A_N^p + \Delta Q_N^p \tag{54}$$

Furthermore, in case of supercritical flow at the outlet, both characteristic equations lead to

$$\Delta A_N^n = \Delta A_N^p, \quad \Delta Q_N^n = \Delta Q_N^p \tag{55}$$

4.4. Local mass conservation (LMC)

This method, proposed by Jin and Fread [10], is based on the use of the discrete form of the mass conservation equation as numerical boundary condition. This leads to

$$[\xi \Delta A_1^n + (1 - \xi)\Delta A_2^n]\delta x + [\theta \delta Q_{(3/2)}^{n+1} + (1 - \theta)\delta Q_{(3/2)}^n]\Delta t = 0$$

$$[\xi \Delta A_N^n + (1 - \xi)\Delta A_{N-1}^n]\delta x + [\theta \delta Q_{N-(1/2)}^{n+1} + (1 - \theta)\delta Q_{N-(1/2)}^n]\Delta t = 0 \tag{56}$$

The parameter $\xi \in [0, 1]$ is a kind of spatial weight and the parameter $\theta \in [0, 1]$ controls the implicitness of the method. The method is of first order except for $\xi = \frac{1}{2}$ that leads to second-order accuracy in space and for $\theta = \frac{1}{2}$, that leads to second-order accuracy in time.

4.5. Semi-explicit mass conservation (SEMC)

The mass equation can be discretized using the semi-explicit upwind scheme (34) at the boundary cells as follows:

$$[(1 + \xi^-)\Delta A^-]_N^n - (\xi^- \Delta A^-)_{N+1}^n = -\frac{\Delta t}{\Delta x}(\delta Q_{N+1}^n - \delta Q_N^n)$$

$$[(1 + \xi^+)\Delta A^+]_1^n - (\xi^+ \Delta A^+)_0^n = -\frac{\Delta t}{\Delta x}(\delta Q_1^n - \delta Q_0^n) \tag{57}$$

where cells 0 and $N + 1$ are exterior to the domain. The variations at those cells are assumed nil, for simplicity,

$$\Delta(A^+)_0^n \approx \Delta(A^-)_{N+1}^n \approx 0 \tag{58}$$

and the value of the discharge at the exterior nodes is estimated as the physical external mass contribution, denoted by ΔM_{in}^n at the inlet and ΔM_{out}^n at the outlet:

$$Q_0^n \Delta t = \Delta M_{\text{in}}^n, \quad Q_{N+1}^n \Delta t = -\Delta M_{\text{out}}^n \tag{59}$$

Hence, the SEMC boundary condition method for the semi-explicit upwind scheme is formulated as

$$\Delta(A^+)_1^n = \frac{\Delta M_{\text{in}}^n - \Delta t Q_1^n}{(1 + \xi_1^+)\Delta x}, \quad \Delta(A^-)_N^n = \frac{\Delta M_{\text{out}}^n + \Delta t Q_N^n}{(1 + \xi_N^-)\Delta x} \tag{60}$$

4.6. Global mass conservation (GMC)

One of the main problems common to all the boundary conditions methods presented up to here is that they always generate some amount of error in the GMC. The GMC, or conservation of the first integral, is an important and desirable property of numerical schemes.

The method of GMC [5, 12] for 1D schemes is based on enforcing the integral form of the mass conservation extended to all the computational domain in combination with a conservative scheme for the interior points to generate the numerical boundary condition. This method is sensitive to the form the mass of the system is evaluated and to the physical boundary conditions.

In a domain discretized using N cells, the total mass is defined as

$$M = \sum_{i=1}^{N} A_i \Delta x \tag{61}$$

so that the mass increment ΔM^n in one time step is

$$\Delta M^n = \sum_{i=1}^{N} \Delta A_i^n \Delta x \tag{62}$$

In a first step, a conservative scheme defined by a nodal flux $\mathbf{F}_i^{\text{T}}$ (as in (31) in the explicit case or (38) in the implicit case) is used all over the domain neglecting contributions from outside cells as in Section 4.3. The cross-section increments predicted in one time step are

$$\Delta A_i^p = -\frac{\Delta t}{\Delta x}(\delta Q_{i+(1/2)}^{\text{R}} + \delta Q_{i-(1/2)}^{\text{L}}) \tag{63}$$

The total numerical mass variation ΔM^p produced by the scheme is therefore:

$$\Delta M^p = \sum_{i=1}^{N} \Delta A_i^p \Delta x = -\Delta t \sum_{i=1}^{N} (\delta Q_{i-(1/2)}^{\text{L}} + \delta Q_{i+(1/2)}^{\text{R}}) = \Delta t(Q_1^{\text{T}} - Q_N^{\text{T}}) \tag{64}$$

Since the scheme used is conservative, this variation is only due to the boundaries and can be split into numerical contribution at the inlet ΔM_{in}^p and at the outlet ΔM_{out}^p in the following form:

$$\Delta M^p = \Delta M_{\text{in}}^p + \Delta M_{\text{out}}^p, \quad \Delta M_{\text{in}}^p = \Delta t Q_1^{\text{T}}, \quad \Delta M_{\text{out}}^p = -\Delta t Q_N^{\text{T}} \tag{65}$$

If the physical boundary condition is, for instance, a certain mass input at the inlet ΔM_{in}^n or at the outlet ΔM_{out}^n, in order to ensure the GMC of the scheme the numerical mass increment must be corrected. This is achieved by means of additional contributions called $\Delta M_{\text{in}}^{\text{a}}$ and $\Delta M_{\text{out}}^{\text{a}}$, so that:

$$\Delta M_{\text{in}}^n = \Delta M_{\text{in}}^{\text{a}} + \Delta M_{\text{in}}^p = \Delta M_{\text{in}}^{\text{a}} + \Delta t Q_1^{\text{T}}$$
$$\Delta M_{\text{out}}^n = \Delta M_{\text{out}}^{\text{a}} + \Delta M_{\text{out}}^p = \Delta M_{\text{out}}^{\text{a}} - \Delta t Q_N^{\text{T}} \tag{66}$$

When using an explicit scheme, the additional mass contributions at the boundaries affect only one cell at each boundary so that the following is proposed:

$$\Delta M_{\text{in}}^{\text{a}} = (A_1^{n+1} - A_1^p)\Delta x, \quad \Delta M_{\text{out}}^{\text{a}} = (A_N^{n+1} - A_N^p)\Delta x \tag{67}$$

Inserting this in (66), the rule defining the GMC method for an explicit scheme is obtained:

$$A_1^{n+1} = A_1^p + \frac{\Delta M_{\text{in}}^n - \Delta t Q_1^{\text{T}}}{\Delta x}, \quad A_N^{n+1} = A_N^p + \frac{\Delta M_{\text{out}}^n + \Delta t Q_N^{\text{T}}}{\Delta x} \tag{68}$$

Within the second-order TVD scheme, inserting the nodal flux (31), this is,

$$A_1^{n+1} = A_1^p + \frac{\Delta M_{\text{in}}^n - \Delta t Q_1^n}{\Delta x}, \quad A_N^{n+1} = A_N^p + \frac{\Delta M_{\text{out}}^n + \Delta t Q_N^n}{\Delta x} \tag{69}$$

When using, on the other hand, implicit schemes, the information must propagate all over the domain for stability reasons. A propagation of the mass contributions at the boundaries can be made in the same form as in the semi-explicit upwind bidiagonal scheme (34):

$$\Delta A_i^{c\pm} = \frac{(\xi \Delta A)_{i\pm1}^{c\pm}}{1 + \xi_i^{\pm}}, \quad \Delta Q_i^{c\pm} = \frac{(\xi \Delta Q)_{i\pm1}^{c\pm}}{1 + \xi_i^{\pm}}$$
$$\Delta A_i^{n+1} = \Delta A_i^p + \Delta A_i^{c+} + \Delta A_i^{c-}, \quad \Delta Q_i^{n+1} = \Delta Q_i^p + \Delta Q_i^{c+} + \Delta Q_i^{c-} \tag{70}$$

Defining the parameters:

$$\tau_1^+ = \tau_N^- = 1, \quad \tau_i^{\pm} = \frac{(\xi \tau)_{i\pm1}^{\pm}}{1 + \xi_i^{\pm}}, \quad \eta^{\pm} = \sum_i \tau_i^{\pm} \tag{71}$$

the following holds:

$$\Delta A_i^{c+} = \tau_i^+ \Delta A_1^{c+}, \quad \Delta A_i^{c-} = \tau_i^- \Delta A_N^{c-} \tag{72}$$

hence

$$\Delta M^{\text{a}} = \sum_i \Delta A_i^{\text{a}} \Delta x = \Delta x \sum_i (\Delta A_i^{c+} + \Delta A_i^{c-})$$
$$= \Delta x \sum_i (\tau_i^+ \Delta A_1^{c+} + \tau_i^- \Delta A_N^{c-}) = \Delta x(\eta^+ \Delta A_1^{c+} + \eta^- \Delta A_N^{c-}) \tag{73}$$

so that the additional mass contributions at the boundaries can be expressed:

$$\Delta M_{\text{in}}^{\text{a}} = \Delta x \eta^+ \Delta A_1^{c+}, \quad \Delta M_{\text{out}}^{\text{a}} = \Delta x \eta^- \Delta A_N^{c-} \tag{74}$$

And, inserting into (66):

$$\Delta A_1^{c+} = \frac{\Delta M_{\text{in}}^n - \Delta t Q_1^{\text{T}}}{\eta^+ \Delta x}, \quad \Delta A_N^{c-} = \frac{\Delta M_{\text{out}}^n + \Delta t Q_N^{\text{T}}}{\eta^- \Delta x} \tag{75}$$

So, finally, the GMC method for the implicit scheme, after applying (75) at the boundaries, propagates the modifications using two bidiagonal steps following (70). In the case of the semi-explicit upwind scheme, using the nodal flux (38), the following two expressions are derived to enable the start of the second sweep:

$$\Delta A_1^{c+} = \frac{\Delta M_{\text{in}}^n - \Delta t Q_1^n - \Delta x (\xi_1^+ \Delta A_1^{p+} - \xi_1^- \Delta A_1^{p-})}{\eta^+ \Delta x}$$

$$\Delta A_N^{c-} = \frac{\Delta M_{\text{out}}^n + \Delta t Q_N^n + \Delta x (\xi_N^+ \Delta A_N^{p+} - \xi_N^- \Delta A_N^{p-})}{\eta^- \Delta x} \tag{76}$$

where ΔA_1^{p+} and ΔA_N^{p-} represent the increments used to start the first sweep of the semi-explicit method. In this method, the choice of the value of these increments is open in the first sweep or predictor step. Either CVE (50) or SEMC (60) can be used for instance. On the other hand, the increments ΔA_1^{p-} and ΔA_N^{p+} are obtained as a result of the completion of the first sweep.

4.7. Subcritical correction

The CVE boundary conditions are independent of the time step size used. However, LMC, SEMC and GMC boundary condition methods depend on that value. For instance, in mass conservation based methods, if an important increase in discharge is imposed upstream and applied in a short time step, these methods may produce only a small variation in the upstream water depth and lead to unrealistic supercritical flows. In that case, at the same time, no numerical information would be extracted from the computational domain. This possibility must be avoided as much as possible. Figure 3, corresponding to Test 1 that will be described later, shows this effect.

   Let us assume that the upstream physical boundary condition is the discharge Q_1^*, and be A_1^{cr} the critical cross section corresponding to that discharge. At the same time, A_1^p represents the cross section predicted by the numerical scheme plus the corresponding numerical boundary condition. The following is proposed:

$$A_1^{n+1} = \max(A_1^p, A_1^{\text{cr}}) \tag{77}$$

If, on the other hand, the physical boundary conditions is the upstream cross section A_1^*, Q_1^{cr} the corresponding critical discharge and Q_1^p the discharge predicted by the numerical scheme plus numerical boundary condition, the following is proposed:

$$Q_1^{n+1} = \min(Q_1^p, Q_1^{\text{cr}}) \tag{78}$$

5. TESTS WITH ANALYTICAL SOLUTION

One of the best forms to study the performance of the numerical schemes is to compare their numerical solution with the analytical solution in problems in which this exists.

5.1. Discontinuous boundary conditions

If a discontinuity is enforced to enter the upstream boundary of an ideal flat and smooth channel of uniform depth and discharge so that the flow properties on both sides obey the
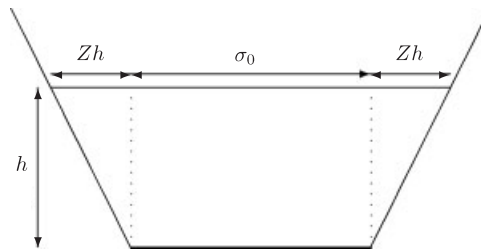

Figure 2. Trapezoidal channel geometry.

Table I. Values of water depth, discharge and shock speed for the test cases of discontinuous boundary conditions.

	Test 1	Test 2
h_i (m)	0.4	0.5
h^* (m)	1	1
Q^* (m^3/s)	24.86021	48.83006
u^* (m/s)	2.486021	4.883006
U (m/s)	4.143385	6.510675
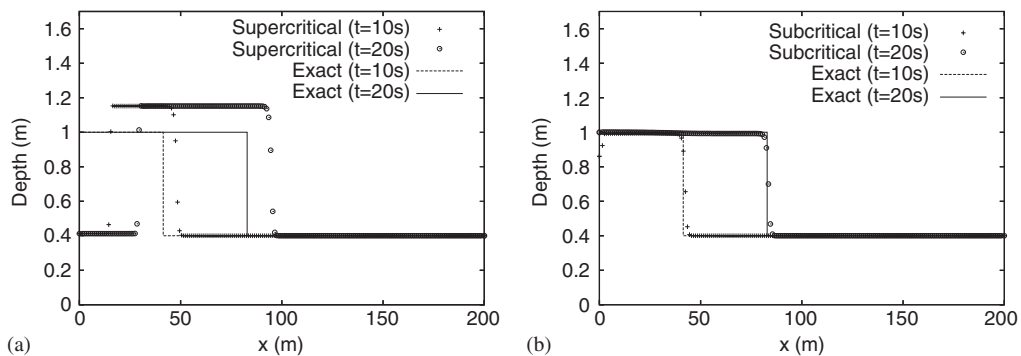
Figure 3. Water depth, imposing discharge at the inlet with the second-order TVD scheme, $\Delta x = 1$ m, CFL $= 0.01$, and GMC: (a) without correction; and (b) with subcritical flow correction.
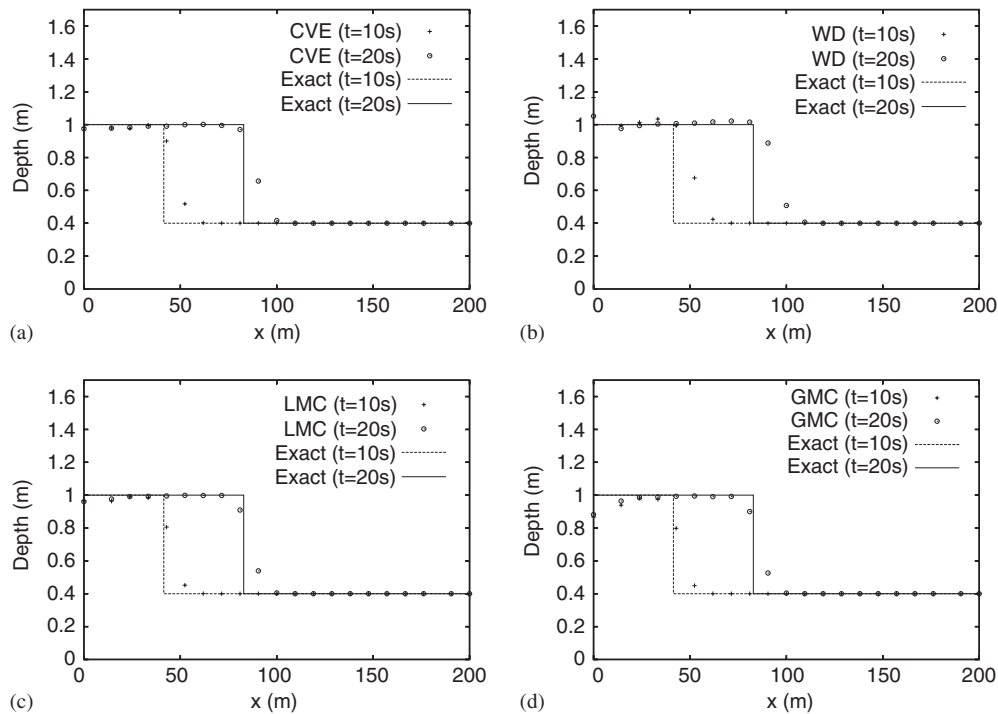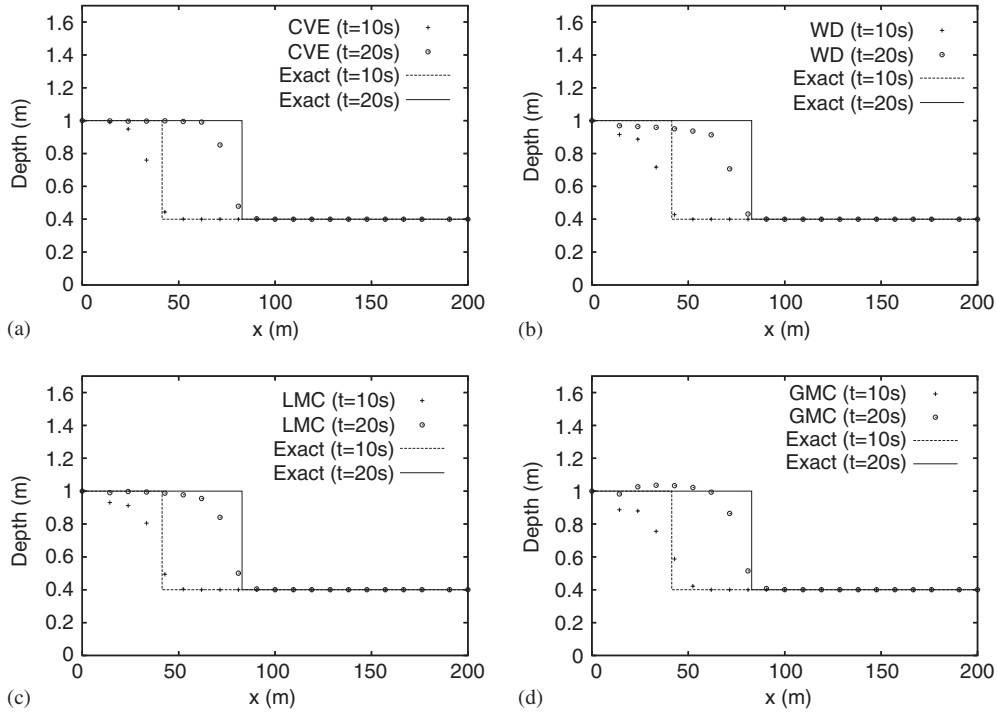
Figure 4. Water depth, imposing the discharge at the inlet, using the second-order TVD scheme, $\Delta x = 10\,\mathrm{m}$, CFL $= 0.9$ and different methods for the upstream numerical boundary condition: (a) first-order spatial CVE; (b) WD; (c) LMC ($\xi = \theta = \frac{1}{2}$); and (d) GMC.

Rankine–Hugoniot equations (17), the discontinuity will propagate unchanged along the channel at a constant speed. From the initial conditions, the water depth h_i and velocity u_i are known in the channel. Imposing h^* or u^* at the boundary, the other variable and the front speed can be worked out from (17). Solving these equations for the discontinuity, we have

$$A^*(u^* - U) = A_i(u_i - U)$$
$$A^*(u^* - U)^2 + gI_{1*} = A_i(u_i - U) + gI_{1i}$$

$$(79)$$

hence,

$$U = u_i + \sqrt{g\frac{A^*}{A_i}\frac{I_{1*} - I_{1i}}{A^* - A_i}}, \quad u^* = U + \frac{A_i}{A^*}(u_i - U), \quad Q^* = A^*u^* \tag{80}$$

In the case of a prismatic trapezoidal channel as in Figure 2, and still-water initial conditions ($u_i = 0$):

$$A = \sigma_0 h + Zh^2, \quad I_1 = \tfrac{1}{2}\sigma_0 h^2 + \tfrac{1}{3}Zh^3 \tag{81}$$

Figure 5. Water depth, imposing the water depth at the inlet, using the second-order TVD scheme, $\Delta x = 10$ m, $CFL = 0.9$ and different methods for the upstream numerical boundary condition: (a) first-order spatial CVE; (b) WD; (c) LMC ($\xi = \theta = \frac{1}{2}$); and (d) GMC.

in that case:

$$U = \sqrt{g \frac{\sigma_0 h^* + Z h^{*2}}{\sigma_0 h_i + Z h_i^2} \frac{\frac{1}{2}\sigma_0(h^{*2} - h_i^2) + \frac{1}{3}Z(h^{*3} - h_i^3)}{\sigma_0(h^* - h_i) + Z(h^{*2} - h_i^2)}}$$

$$u^* = U - \frac{\sigma_0 h_i + Z h_i^2}{\sigma_0 h^* + Z h^{*2}} U, \quad Q^* = [\sigma_0(h^* - h_i) + Z(h^{*2} - h_i^2)]U \tag{82}$$

This solution gets much simpler in the case of a rectangular section:

$$U = \sqrt{g \frac{h^*}{h_i} \frac{h^* + h_i}{2}}, \quad u^* = \left(1 - \frac{h_i}{h^*}\right)U, \quad Q^* = \sigma_0(h^* - h_i)U \tag{83}$$

or triangular:

$$U = \sqrt{\frac{g}{3} \frac{h^{*2}}{h_i^2} \frac{(h^{*3} - h_i^3)}{(h^{*2} - h_i^2)}}, \quad u^* = \left[1 - \left(\frac{h_i}{h^*}\right)^2\right]U, \quad Q^* = Z(h^{*2} - h_i^2)U \tag{84}$$
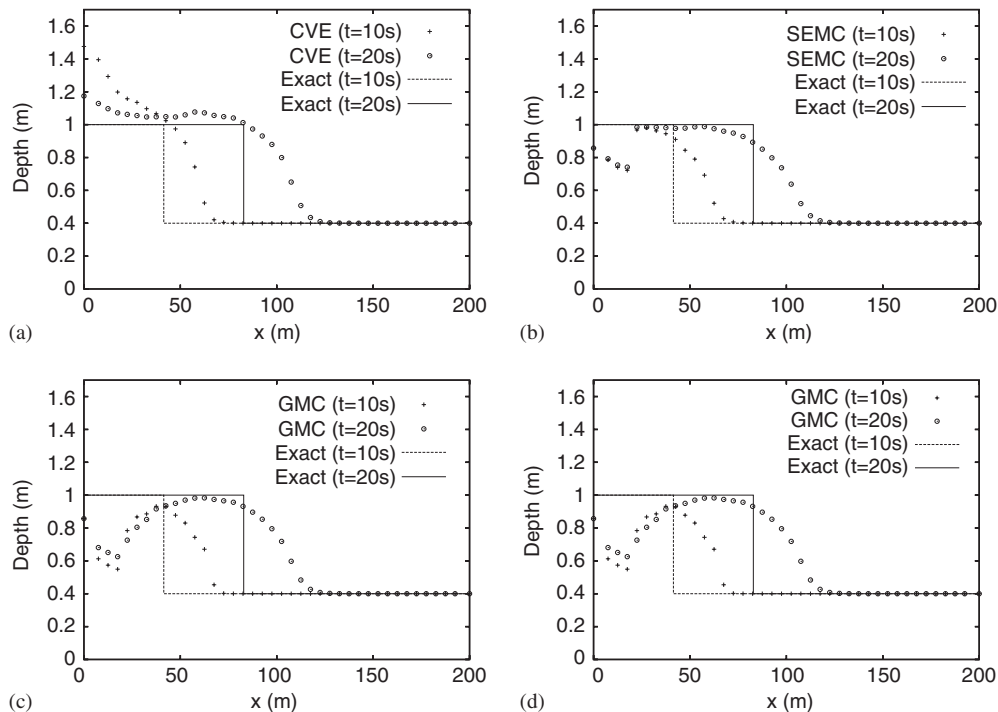
Figure 6. Water depth, imposing the discharge at the inlet, using the first-order semi-explicit upwind scheme, $\Delta x = 5$ m, CFL $= 4$ and the numerical boundary condition methods: (a) zero-order temporal CVE; (b) SEMC; (c) GMC with CVE in the predictor step; and (d) GMC with SEMC in the predictor step.

Two test cases are next proposed to study the accuracy of the resulting combinations of proposed numerical schemes for the interior points and methods for the numerical boundary conditions. First, the propagation of a non-transcritical discontinuity in a rectangular channel ($\sigma = 10$ m) and, second, the propagation of a transcritical discontinuity in a triangular channel ($Z = 10$). The details of both test cases are gathered in Table I. The mass error produced in each case will be computed as follows:

$$E_{\text{mass}} = 100 \frac{|M_{\text{exact}} - M_{\text{numerical}}|}{M_{\text{exact}}} \%$$

5.1.1. Test 1: Subcritical case. In Figure 3 the second-order explicit TVD scheme and the GMC method with and without subcritical correction are applied to Test 1. The results have been obtained using a uniform grid of $\Delta x = 1$ m in order to avoid numerical diffusion as much as possible. In Figure 3(a) the GMC method devoid of correction generates a very low water depth at the inlet, hence unphysical supercritical flow that gives rise to a moving hydraulic jump to connect with the downstream conditions.
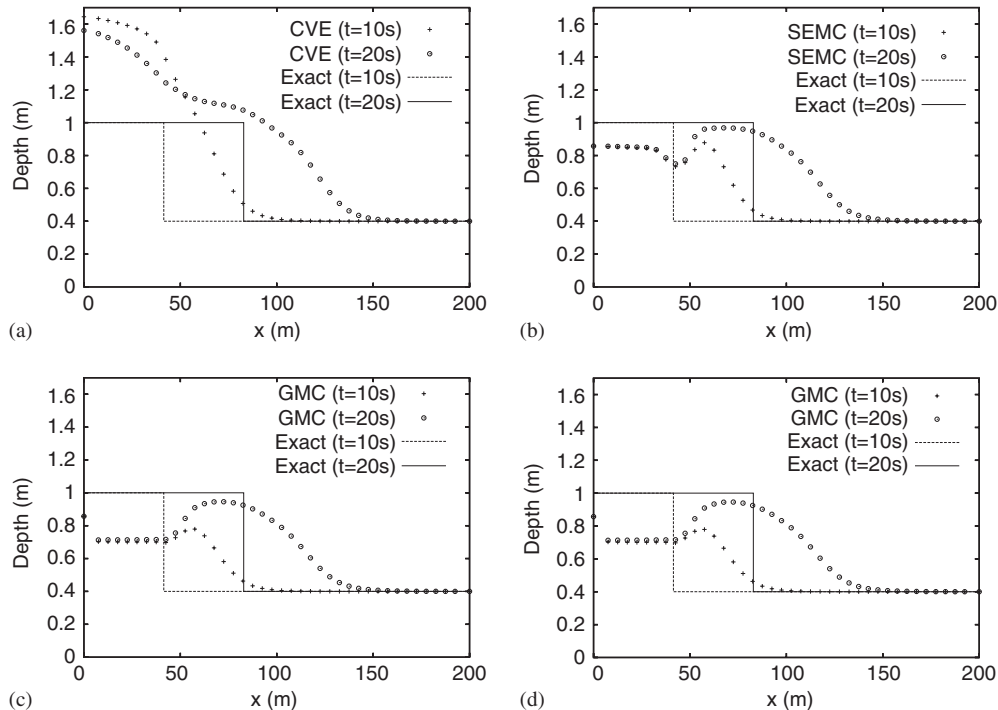
Figure 7. Water depth, imposing the discharge at the inlet, using the first-order semi-explicit upwind scheme, $\Delta x = 5\,\text{m}$, $\text{CFL} = 10$ and the numerical boundary condition methods: (a) zero-order temporal CVE; (b) SEMC; (c) GMC with CVE in the predictor step; and (d) GMC with SEMC in the predictor step.

Figures 4 and 5 display the numerical results obtained in Test 1 imposing, respectively, discharge and water depth at the upstream boundary and using the second-order explicit TVD scheme and four different approaches for the discretization of the upstream numerical boundary condition. A uniform grid of $\Delta x = 10\,\text{m}$ was used in order to be able to identify the different solutions. The plots show only slight visual differences among the different methodologies. It can be remarked that the WD method is the less accurate and the spatial first-order CVE the less oscillatory; however, the GMC is the only method achieving a reduction in the mass error to machine precision.

Figures 6–9 are a plot of the numerical results from the semi-explicit upwind scheme using four different approaches for the discretization of the upstream numerical boundary condition. Figures 6 and 7 correspond to the case of imposing the upstream discharge and display the results of using, respectively, $\text{CFL} = 4$ and 10. Figures 8 and 9 correspond to the case of imposing the upstream water depth and display the results of using, respectively, $\text{CFL} = 4$ and 10. A uniform grid of $\Delta x = 5\,\text{m}$ was used in order to reduce the numerical diffusion. It can be seen that, in general, the solution in presence of discontinuous boundary conditions using this scheme is less accurate than using the explicit scheme. If the interest is put on the front tracking detail, these solutions can be considered unacceptable. The solution is almost
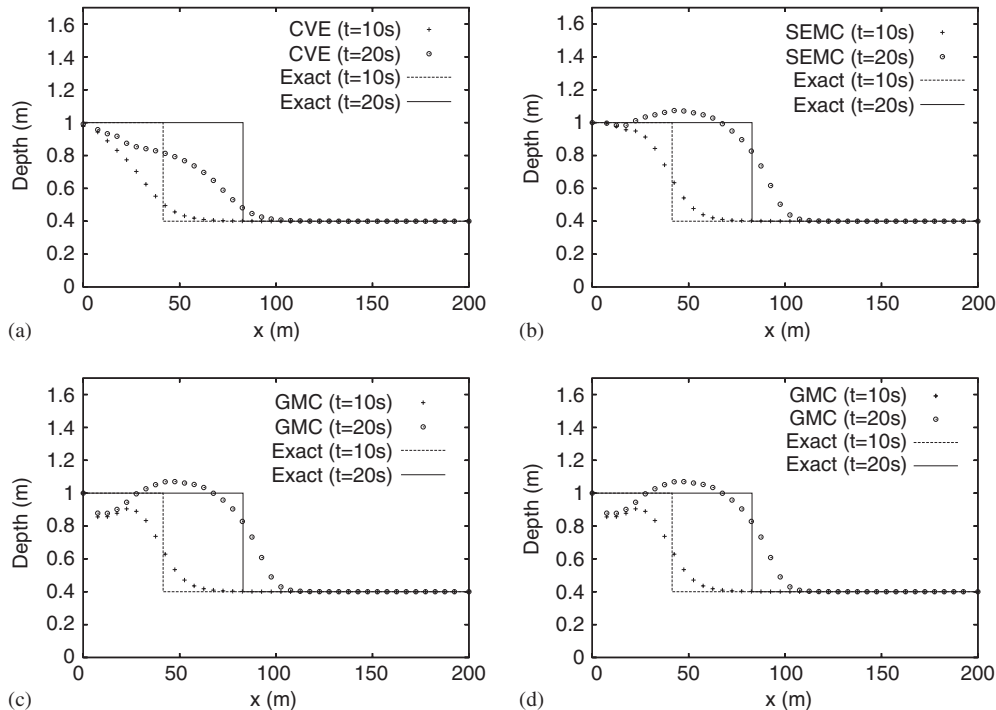
Figure 8. Water depth, imposing the water depth at the inlet, using the first-order semi-explicit upwind scheme, $\Delta x = 5\,\text{m}$, CFL $= 4$ and the numerical boundary condition methods: (a) zero-order temporal CVE; (b) SEMC; (c) GMC with CVE in the predictor step; and (d) GMC with SEMC in the predictor step.

identical when the GMC correction is applied to both predictor approaches, the spatial zero-order CVE method or the SEMC technique. Despite the visual similarity among the solutions, this correction is the only method leading to an exact mass conservation. Between the two predictor options, the results show that the CVE leads to the worst solution (Tables II and III).

5.1.2. Test 2: Supercritical case. Figure 10 contains several discharge and water depth plots of the solutions obtained for Test 2 using the two numerical schemes considered at different times. As the inlet flow is supercritical, two upstream physical boundary conditions are imposed and no upstream numerical boundary conditions are present. The numerical solution provided by the semi-explicit scheme is more accurate in this case than in the subcritical inflow test case for all CFL values due to the fact that both variables, discharge and water depth, are imposed simultaneously. However, as there is no freedom to enforce the global conservation, a non zero mass error is introduced in the solution in all cases (see Table IV).

5.2. Steady flow in a channel

MacDonald [24, 25] derived and proposed several steady open channel flow test cases with analytical solution. All of them involved variable bottom level and bed friction. In order to
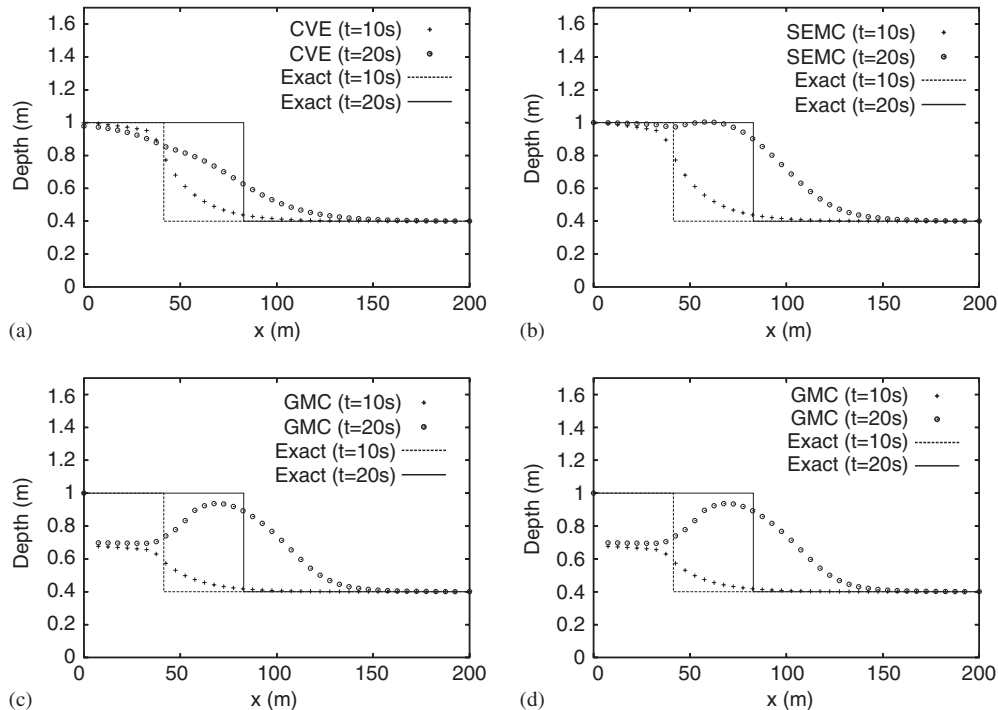
Figure 9. Water depth, imposing the water depth at the inlet, using the first-order semi-explicit upwind scheme, $\Delta x = 5\,\mathrm{m}$, CFL $= 10$ and the numerical boundary condition methods: (a) zero-order temporal CVE; (b) SEMC; (c) GMC with CVE in the predictor step; and (d) GMC with SEMC in the predictor step.

Table II. Percentage mass error, imposing discharge or water depth at the inlet, produced after $20\,\mathrm{s}$ by the different numerical boundary condition methods using the second-order TVD scheme with $\Delta x = 10\,\mathrm{m}$ and CFL $= 0.9$.

	Discharge	Water depth
CVE	2.46	3.07
WD	5.33	4.14
LMC	1.05	2.90
GMC	0	0

check the influence of the numerical boundary condition method adopted on the steady flow solution, one of them has been selected. It is a rectangular cross-section prismatic channel $150\,\mathrm{m}$ long and $10\,\mathrm{m}$ wide where a discharge of $20\,\mathrm{m}^3/\mathrm{s}$ flows in subcritical regime. The value of the Manning roughness is $0.03\,\mathrm{m}^{-1/3}\mathrm{s}$ and the steady water depth follows:

$$h = 0.8 + 0.25 \exp\left[-33.75\left(\frac{x - 75}{150}\right)^2\right] \qquad (85)$$

Table III. Percentage of mass error produced by the different numerical boundary condition methods and the first-order semi-explicit method, imposing discharge or water depth at the inlet, after 20 s.

	CFL = 4		CFL = 10	
	Discharge	Water depth	Discharge	Water depth
CVE	53.07	40.99	121.24	85.85
SEMC	76.98	68.64	70.87	65.80
GMC (CVE)	0	0	0	0
GMC (SEMC)	0	0	0	0

Table IV. Percentage of mass error produced by the second-order TVD scheme with $\Delta x = 10$ m and CFL = 0.9 and the first-order semi-explicit scheme with $\Delta x = 5$ m, and with CFL = 4 and 10 after 20 s.

	Mass error (%)
TVD (CFL = 0.9)	0.89
Semi-explicit (CFL = 4)	1.52
Semi-explicit (CFL = 10)	2.20

The bottom level can be calculated from the slope that, according to (1), is

$$S_0 = S_f + \frac{\partial h}{\partial x} - \frac{Q^2}{gA^3} \frac{\partial A}{\partial x} \qquad (86)$$

In Figure 11 the exact longitudinal profiles of water depth, water level and bottom level have been plotted.

Figures 12–15 display the solutions obtained with the different methods. It is worth noting that, although important differences were found in the discontinuous unsteady cases, all the methods considered here, both for interior points as well as for numerical boundary conditions, lead to identical results in the steady case. The reason is that this example represents a very different kind of flow and is much less challenging for the numerical method at the boundaries. In this case, the solution is determined by the numerical scheme used for the interior points and the treatment of the source terms. The exact conservation of the steady discharge is a direct consequence of the non-pointwise discretization of the source terms [4].

6. RIVER FLOW APPLICATION: ÉSERA RIVER

Ésera River is a Spanish river on the left bank of the Ebro River basin. It flows through a touristic mountain area of the Pirynees. A study has been carried on led by the interest to evaluate the risk of inundation in a few nearby camping sites. It is a typical, irregular and sloping mountain river (average slope around 4%, Figure 16(a)). Thirty-two measured cross sections were used to define the 1 km long river reach bed form, a base discharge of $10 \, \text{m}^3/\text{s}$
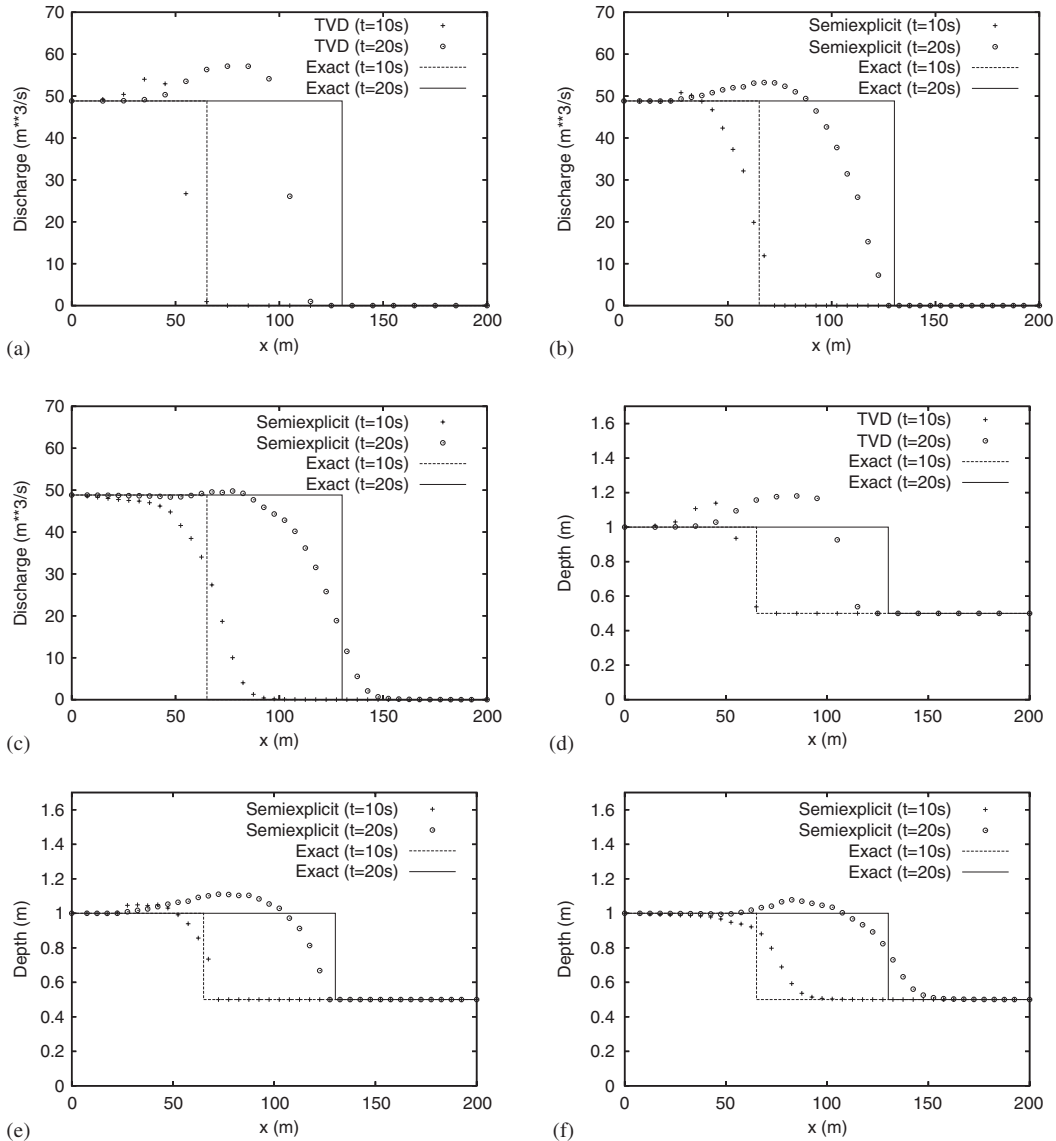
Figure 10. (a), (b) and (c) discharge; (d), (e) and (f) water depth: with the schemes (a) and (d) second-order TVD with $\Delta x = 10$ m and CFL $= 0.9$, (b), (c), (e) and (f) first-order semi-explicit with $\Delta x = 5$ m, (b), (e) CFL $= 4$, (c) and (f) CFL $= 10$.

to state the initial flow conditions, and a high roughness Manning coefficient $n = 0.031$ m$^{-1/3}$s to model the stony bed of average stone diameter 20 cm, according to Strickler [26].

Four flooding discharges of 236, 344, 414 and 563 m^3/s, corresponding to return periods 10, 50, 100 and 500 year, respectively, were assumed in the study. Due to the lack of gauging points and the sloping character of the river bed, a critical flow condition was assumed at
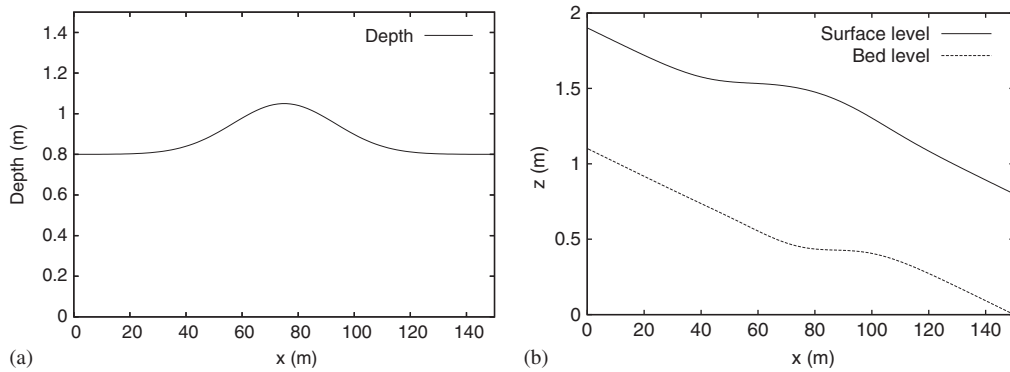
Figure 11. Steady longitudinal profiles. MacDonald's test: (a) water depth; and (b) surface level and bottom level.
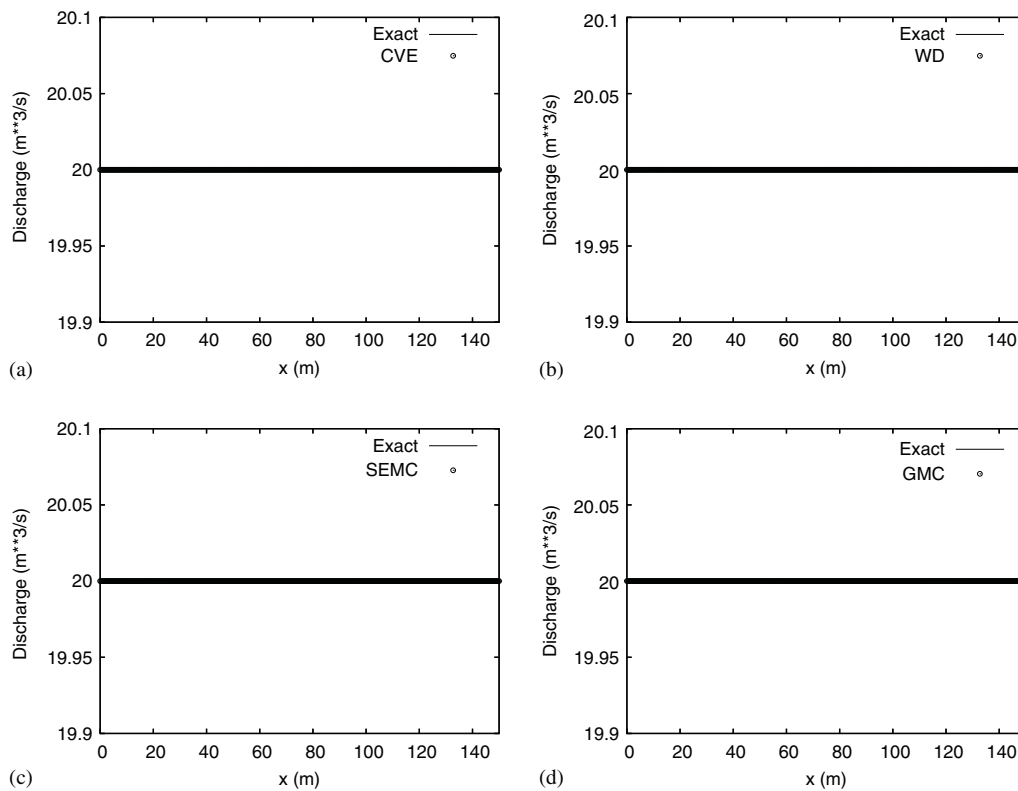

Figure 12. Discharge in the MacDonald's test case with the second-order TVD scheme, $\Delta x = 0.375$ m, CFL $= 0.9$ and the numerical boundary condition methods: (a) first-order spatial CVE; (b) WD; (c) LMC ($\xi = \theta = \frac{1}{2}$); and (d) GMC.
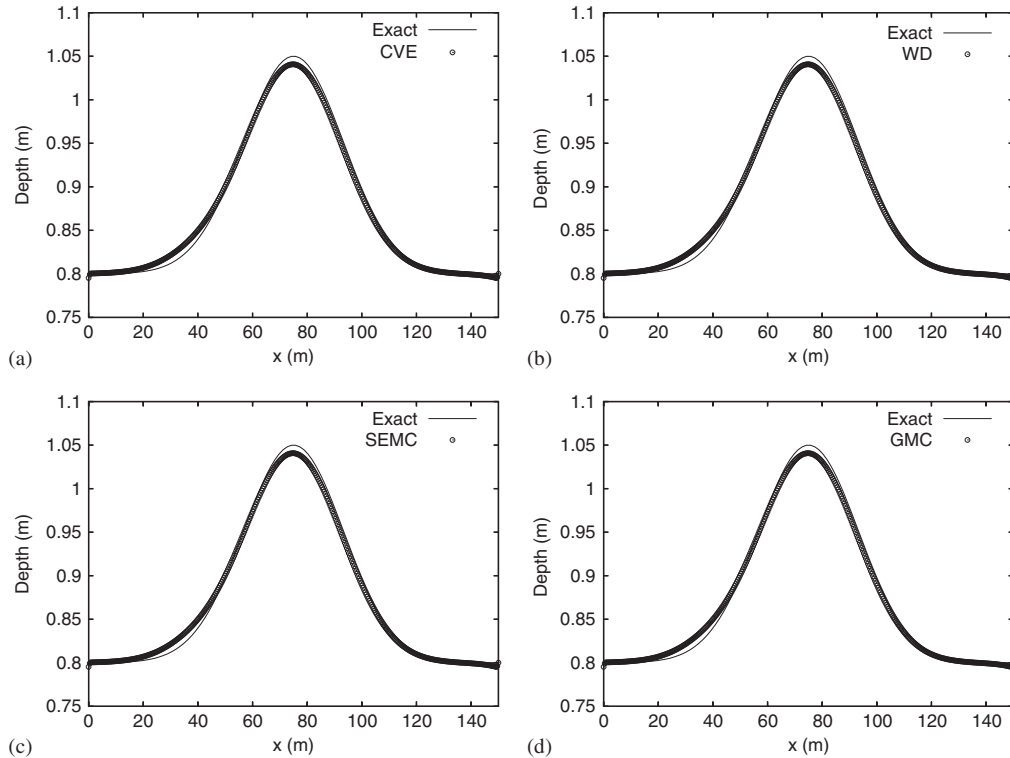
Figure 13. Water depth in the MacDonald's test case with the
second-order TVD scheme, $\Delta x = 0.375$ m, CFL $= 0.9$ and the
numerical boundary condition methods: (a) first-order spatial
CVE; (b) WD; (c) LMC ($\xi = \theta = \frac{1}{2}$); and (d) GMC.

the inlet in all these cases. There was no field information either at the reach outlet so that a critical outflow condition was assumed in case of downstream subcritical flow. At the upstream boundary, the GMC method (with SEMC predictor step in the semi-explicit scheme) was used for the numerical condition discretization together with the subcritical flow correction.

The calculation was performed in two steps. In a first step, the steady base flow was determined by sudden introduction of the base discharge over dry bed initial conditions. After convergence, this led to the initial conditions for the second run. Figure 16(b) is a plot of the water depth profiles corresponding to the base flow discharge and the four inundation discharges all flowing in steady state as computed with the second-order TVD explicit scheme. Note the distorted scale in the figure.

Figure 17 is a comparison of the numerical results provided by the two numerical schemes considered in this paper for the first run. They contain three snapshots of the transient solution generated by the discontinuous boundary condition over initial dry bed. It is important to remark that the semi-explicit scheme is able to supply a solution almost identical to the explicit scheme using a CFL ten times bigger. The total CPU time used by the two schemes
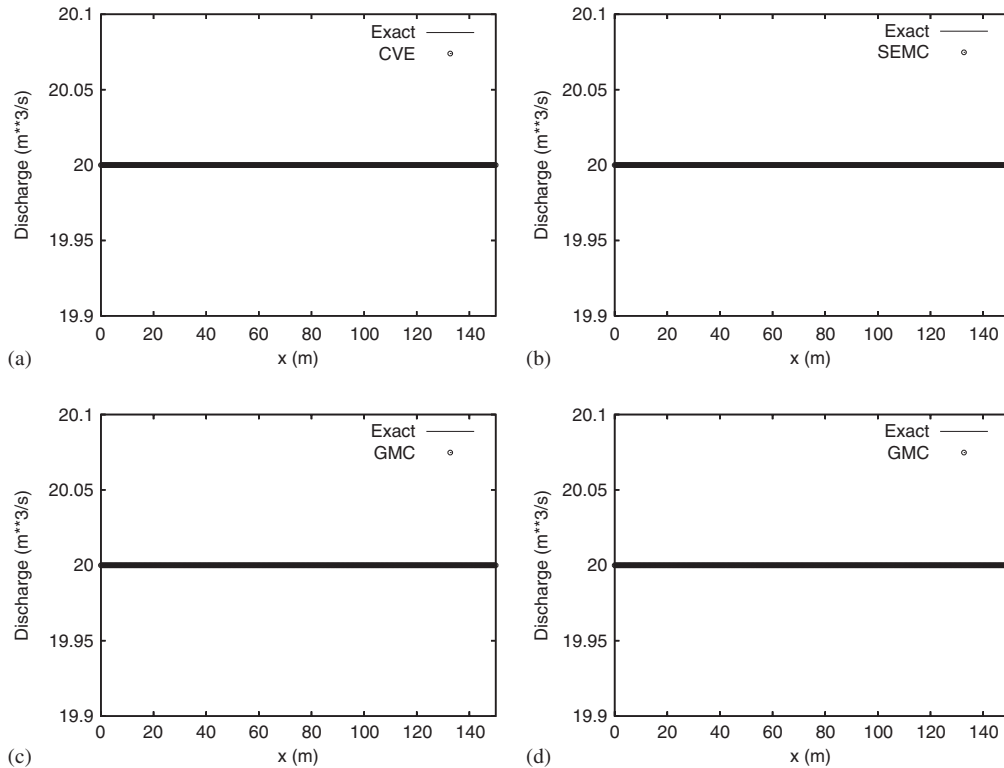
Figure 14. Discharge in the MacDonald's test case with the upwind semi-explicit scheme, $\Delta x = 0.375$ m, CFL $= 10$ and the numerical boundary condition methods: (a) zero-order temporal CVE; (b) SEMC; (c) GMC with CVE in the predictor step; and (d) GMC with SEMC in the predictor step.

was 17 s in the explicit case and 2 s in the semi-explicit case in a AMD Athlon 2600 laptop computer.

Figure 18 is a comparison of the numerical results provided by the two numerical schemes considered in this paper for the calculation of the advance of the 500 year discharge introduced as a discontinuous boundary condition. They contain three snapshots of the transient solution over the initial base flow conditions. The semi-explicit scheme is able to supply a solution to this exacting unsteady flow case even using a CFL $= 100$. During the advance phase, the semi-explicit solution is more diffusive than the explicit solution but they are identical when the steady state is reached. The total CPU time used by the two schemes was 26 s in the explicit case and 0.3 s in the semi-explicit case in the same computer.

7. CONCLUSIONS

This paper is a contribution to the improvement of fully conservative methods for conservation laws. The emphasis has been put on the fact that, apart from a good conservative scheme for
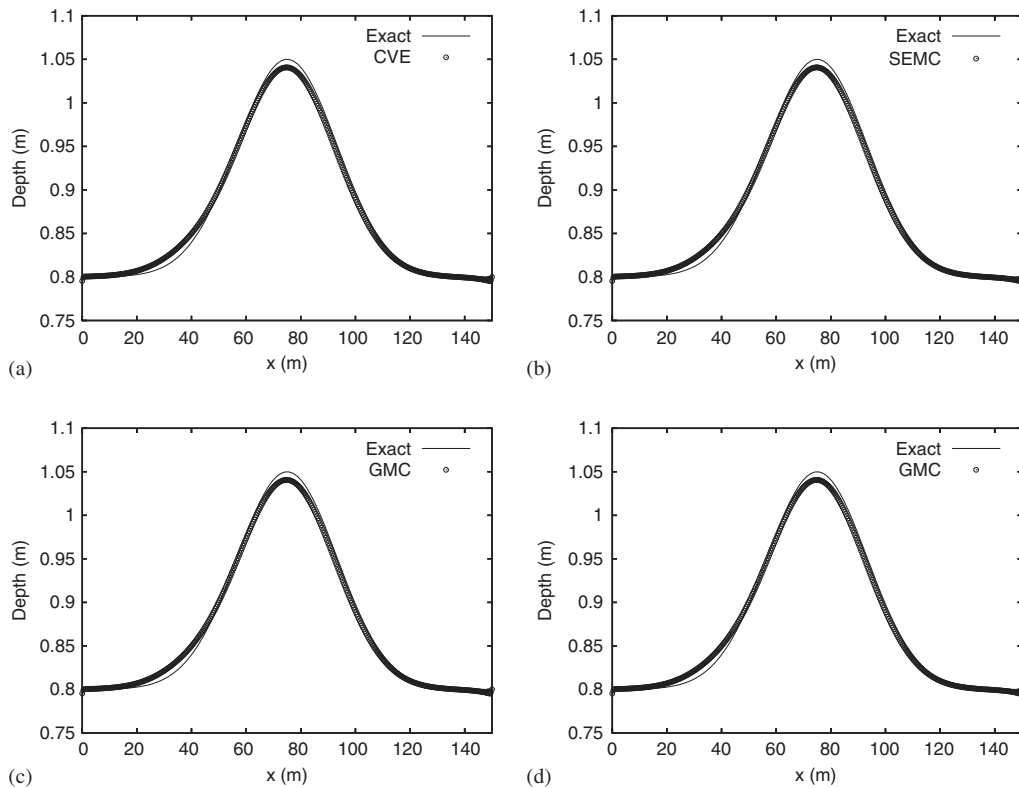
Figure 15. Water depth in the MacDonald's test case with the upwind semi-explicit scheme, $\Delta x = 0.375\,\text{m}$, $\text{CFL} = 10$ and the numerical boundary condition methods: (a) zero-order temporal CVE; (b) SEMC; (c) GMC with CVE in the predictor step; and (d) GMC with SEMC in the predictor step.
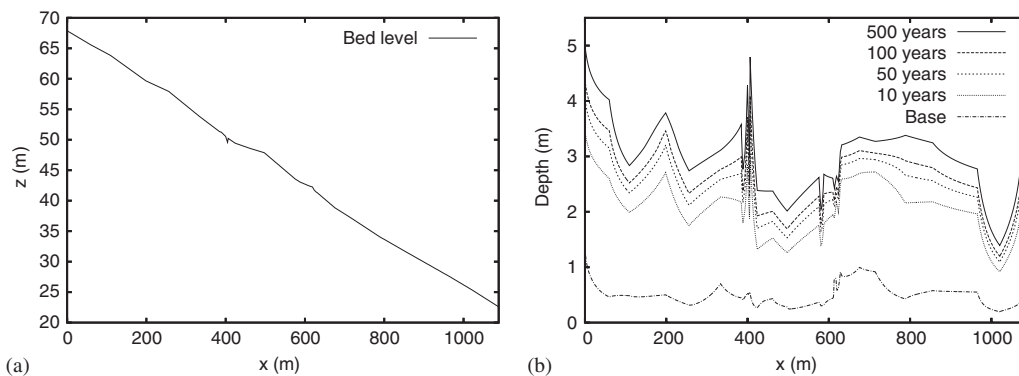

Figure 16. Longitudinal bed level profile in the Esera River reach (a) and several steady flow water depth profiles; and (b) as obtained from the second-order TVD scheme using $\Delta x = 1\,\text{m}$ and $\text{CFL} = 0.9$.
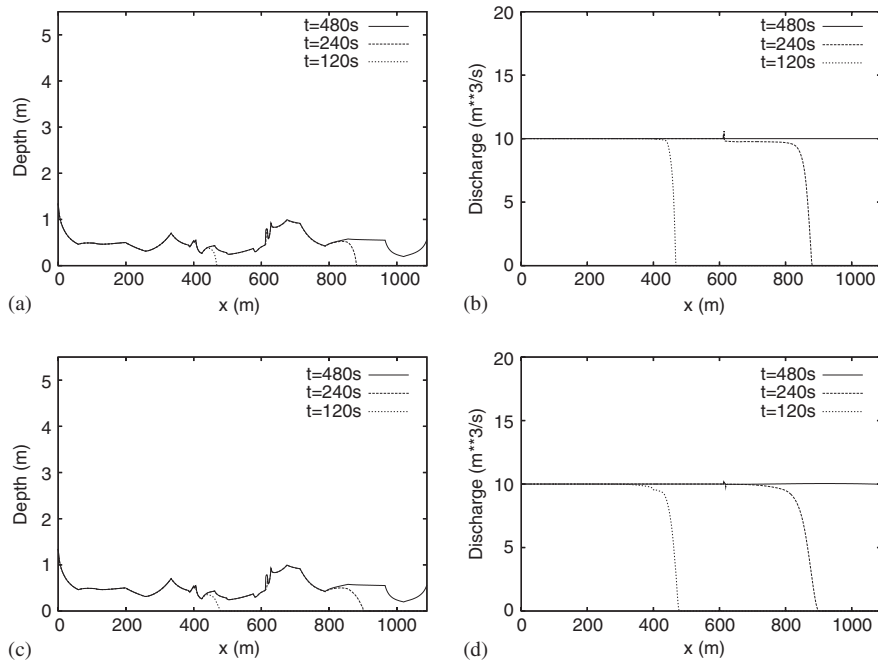
Figure 17. Longitudinal profiles of water depth (a), (c) and discharge (b), (d) in the Ésera River at three times after the sudden introduction of the base discharge over dry bed initial conditions. (a), (b) using second-order TVD explicit scheme with CFL = 0.9 and (c), (d) using upwind semi-explicit scheme with CFL = 10. $\Delta x = 1$ m.

the interior points and a correct discretization of the source terms, it is important to know which are the best options for the treatment of the boundary conditions. A revision of the most widely used methods of discretization of the numerical boundary conditions has been supplied and a different method, based on the conservation of the integral of the mass over the whole domain, has been also considered. In order to quantitatively compare the results provided by the different methods, two new test cases of unsteady discontinuous flow with analytical solution have been proposed.

All the methods considered for the numerical boundary condition discretization are able to solve accurately unsteady flow with discontinuities at the boundary when combined with explicit schemes for the interior points. However, only the GMC method leads to an exactly conservative solution. When combined with a two-step semi-explicit method using high CFL values the results are less accurate in general. Even with the loss of accuracy, global mass conservation is achieved only if the GMC method is implemented. In all cases, the necessity to include a subcritical correction at the inlet has been detected mainly when using small time steps.

In cases of steady flow, the GMC method does not improve the quality of the solutions over that of other options among those considered here. The GMC method has also been applied to a full-scale case of unsteady river flow leading to very satisfactory results both
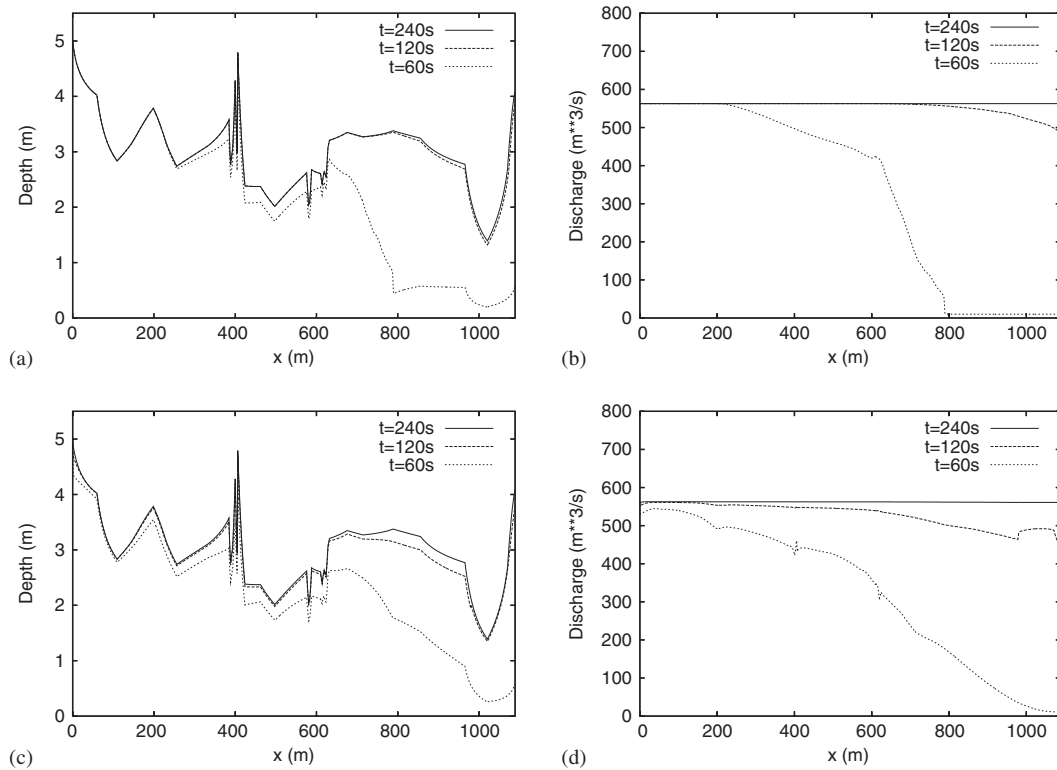
Figure 18. Longitudinal profiles of water depth (a), (c) and discharge (b), (d) in the Ésera River at three times after the sudden introduction of the 500 year return period discharge over base flow initial conditions. (a), (b) using second-order TVD explicit scheme with $CFL = 0.9$ and (c), (d) using upwind semi-explicit scheme with $CFL = 100$. $\Delta x = 1$ m.

in combination with the explicit and the semi-explicit scheme. When using the semi-explicit scheme, accurate and conservative solutions have been obtained using $CFL = 100$.

The GMC method described can be adapted to any conservative method used for the interior points. It is simple and able to provide fully conservative numerical solutions in presence of both steady and unsteady continuous or discontinuous solutions.

REFERENCES

1. Glaister P. Approximate Riemann solutions of the shallow water equations. *Journal of Hydraulic Research* 1988; **26**:293–306.
2. García Navarro P, Vázquez Cendón ME. Some considerations and improvements on the performance of Roe's schemes for 1D irregular geometries on numerical treatment of the source terms in the shallow water equations. *Computers and Fluids* 2000; **126**:26–40.
3. Burguete J, García Navarro P. Efficient construction of high-resolution TVD conservative schemes for equations with source terms: application to shallow water flows. *International Journal for Numerical Methods in Fluids* 2001; **37**:209–248.
4. Burguete J, García Navarro P. Improving simple explicit methods for unsteady open channel and river flow. *International Journal for Numerical Methods in Fluids* 2004; **45**:125–156.

5. Burguete J, García Navarro P. Implicit schemes with large time step for non-linear equations: application to river flow hydraulics. *International Journal for Numerical Methods in Fluids* 2004; **46**:607−636.
6. Kreiss HO. Initial boundary value problem for hyperbolic systems. *Communication of Pure and Applied Mathematics* 1970; **23**:277−298.
7. Fox L. *Numerical Solution of Ordinary and Partial Differential Equations.* Pergamon Press: New York, 1962.
8. Yee HC. Numerical approximation of boundary conditions with applications to inviscid equations of gas dynamics. *NASA Technical Memorandum 81265*, 1981.
9. Yee HC, Beam RM, Warming RF. Boundary approximations for implicit schemes for one-dimensional inviscid equations of gas dynamics. *AIAA Journal* 1982; **20**(9):1203−1211.
10. Jin M, Fread DL. Dynamic flood routing with explicit and implicit numerical solution schemes. *Journal of Hydraulic Engineering* (ASCE) 1997; **123**(3):166−173.
11. Villanueva I. Estudio de regímenes transitorios y permanentes en ríos y canales. *Ph.D. Thesis*, University of Zaragoza, 1999.
12. Burguete J, García Navarro P, Aliod R. Numerical simulation of runoff from extreme rainfall events in a mountain water catchment. *Natural Hazards in Earth System Sciences* 2002; **2**:1−9.
13. Saint Venant AJCB de. Théory de mouvement non-permanent des eaux avec aplication aux crues de rivières et á l'introduction des marées dans leur lit. *Comptes Rendus de l'Académie des Sciences*, *Paris*, 1871.
14. Gauckler PG. Études théoriques et practiques sur l'écoulement et le mouvement des eaux. *Comptes Rendus de l'Académie des Sciences*, *Paris*, 1867.
15. Manning R. *On the Flow of Water in Open Channels and Pipes*. Institution of Civil Engineers of Ireland, 1890.
16. Hirsch C. *Computational Methods for Inviscid and Viscous Flows*: *Numerical Computation of Internal and External Flows*. Wiley: New York, 1990.
17. Roe PL. Approximate Riemann solvers, parameter vectors, and difference schemes. *Journal of Computational Physics* 1981; **43**(2):357−372.
18. Sweby PK. High resolution schemes using flux limiters for hyperbolic conservation laws. *SIAM Journal on Numerical Analysis* 1984; **21**:995−1011.
19. Roe PL. Generalized formulation of TVD Lax–Wendroff schemes. *ICASE Report 84-53*, *NASA CR-172478*, NASA Langley Research Center, 1984.
20. Courant R, Friedrichs KO, Lewy H. Über die partiellen Differenzengleichungen der mathematisches. *Mathematische Annalen* 1928; **100**:32−74.
21. Gustafsson B. The convergence rate for difference approximations to mixed initial boundary value problem. *Mathematics of Computations* 1975; **29**:396−406.
22. Kreiss HO. Difference approximations for mixed initial boundary value problems. *Proceedings of the Royal Society of London Series A* 1971; **323**:255−261.
23. Gustafsson B, Kreiss HO, Sundström A. Stability theory of difference approximations for mixed initial boundary value problems. *Mathematics of Computations* 1972; **26**:649−686.
24. MacDonald I. Analysis and computation of steady open channel flow. *Ph.D. Thesis*, University of Reading, 1996.
25. MacDonald I, Baines MJ, Nichols NK, Samuels PG. Analytical benchmark solutions for open-channel flows. *Journal of Hydraulic Engineering* (ASCE) 1997; **123**(11):1041−1045.
26. Strickler A. *Beiträge zur Frage der Geschwindigkeitsformel und der Rauhligkeitszahlen für Ströme, Kanäle und Geschlossene Leitungen*. Mitt. des Eidgenössischen Amtes für Wasserwirtschaft: Bern, vol. 16, 1923.